

# Double Temporal Sparsity Based Accelerated Reconstruction of Compressively Sensed Resting-State fMRI

Priya Aggarwal<sup>a,\*</sup>, Anubha Gupta<sup>a</sup>

<sup>a</sup>*Signal processing and Bio-medical Imaging Lab, Department of Electronics and Communication Engineering, Indraprastha Institute of Information Technology (IIIT), Delhi, India*

---

## Abstract

A number of reconstruction methods have been proposed recently for accelerated functional Magnetic Resonance Imaging (fMRI) data collection. However, existing methods suffer with the challenge of greater artifacts at high acceleration factors. This paper addresses the issue of accelerating fMRI collection via undersampled  $k$ -space measurements combined with the proposed method based on  $l^1 - l^1$  norm constraints, wherein we impose first  $l^1$ -norm sparsity on the voxel time series (temporal data) in the transformed domain and the second  $l^1$ -norm sparsity on the successive difference of the same temporal data. Hence, we name the proposed method as Double Temporal Sparsity based Reconstruction (DTSR) method. The robustness of the proposed DTSR method has been thoroughly evaluated both at the subject level and at the group level on real fMRI data. Results are presented at various acceleration factors. Quantitative analysis in terms of Peak Signal-to-Noise Ratio (PSNR) and other metrics, and qualitative analysis in terms of reproducibility of brain Resting State Networks (RSNs) demonstrate that the proposed method is accurate and robust. In addition, the proposed DTSR method preserves brain networks that are important for studying fMRI data. Compared to the existing methods, the DTSR method shows promising potential with an improvement of 10-12dB in PSNR with acceleration factors upto 3.5 on resting state fMRI data. Simulation results on real data demonstrate that DTSR method can be used to acquire accelerated fMRI with accurate detection of RSNs.

*Keywords:* Accelerated functional MRI,  $l^1$  minimization, sparse recovery, compressed sensing,  $k$ - $t$  acceleration, undersampling.

---

\*Corresponding author

*Email addresses:* priyaa@iiitd.ac.in (Priya Aggarwal), anubha@iiitd.ac.in (Anubha Gupta)

## 1. Introduction

Functional Magnetic Resonance Imaging (fMRI) is a prominent and widely used noninvasive neuroimaging modality [1, 2, 3]. It is used to understand brain functions by measuring Blood Oxygen Level Dependent (BOLD) signals. BOLD fMRI signals are captured via T2\* weighted imaging. Achieving high temporal resolution remains challenging in fMRI. In addition, one of the major challenges in fMRI is the low sensitivity of BOLD signals leading to images blurred with motion and other artifacts. Poor sensitivity of BOLD signals leads to lower Signal-to-Noise Ratio (SNR). Moreover, long scanning times lead to annoyance in patients. Hence, there is a need to capture images in the shortest possible time.

Various remedies have been proposed to address high spatio-temporal resolution of fMRI such as development of high magnetic field scanner [4, 5, 6, 7], coil sensitivity improvement inside fMRI scanner [8], advancements in pulse sequences [9, 10], usage of parallel imaging [11, 12], and compressed sensing (CS) based fMRI reconstruction from fewer  $k$ -space (spatial Fourier domain) measurements [13, 14, 15, 16, 17, 18, 19, 20, 21, 22]. In this paper, we address the problem of accelerated fMRI reconstruction without the loss of BOLD sensitivity in the CS framework.

Compressive sampling involves capturing of less data [23]. Since acquisition time is directly related to the number of measurements, CS reduces the data acquisition time in fMRI. CS allows reconstruction of fMRI brain volumes using less number of  $k$ -space measurements that are picked up at a sampling rate lower than the Nyquist sampling rate, provided some assumptions hold true. In general, it is assumed that the data is sparse in some transform domain and that the chosen samples are incoherent [15]. Compressive sensing framework helps in fMRI reconstruction in two significant ways: 1) It helps in increasing the statistical power of the BOLD signal [16, 19] because of its inherent denoising property and 2) it provides improvement in the spatiotemporal resolution of fMRI data [17, 21, 13, 22, 14, 18, 20, 15, 24, 25].

Various CS based reconstruction methods have been proposed so far for accelerated fMRI reconstruction [13, 14, 15, 16, 17, 18, 19, 20, 21, 22, 25, 24]. These methods can be largely divided into two categories. First category includes on-line methods that reconstruct fMRI data in real time [13, 14, 15, 16, 17]. These methods reconstruct brain volume at time  $t$  using the volume at time  $t - 1$  by assuming causality in the reconstruction framework. Second category includes offline methods that first store  $k$ -space data of all fMRI volumes and later, utilize this complete information across both time and space, also called  $k$ - $t$  space data, to reconstruct fMRI data [18, 19, 20, 21, 22, 25, 24].

Many offline reconstruction methods, such as Compressed sensing with wavelet domain sparsity (CSWD) [19], HSPARSE [20],  $k$ - $t$  FASTER [21], and LR+S [22], have been proposed in the fMRI literature. These methods largely differ in regularization constraints in CS fMRI reconstruction framework. CS fMRI solves a set of underdetermined equations that has infinitely many solutions. In order to recover a unique solution corresponding to the signal of interest,

regularization constraints are added. Often, sparsity in some transform domain is added as the regularization constraint. Theoretical studies have shown that it is possible to recover sparse signals by  $l^1$  norm minimization [26].

For example, in [19], undersampled fMRI data is reconstructed using compressed sensing with sparsity of fMRI data in the wavelet domain, wherein orthogonal Daubechies wavelet is used as the sparsifying basis. In [19], fMRI data is reconstructed using  $l^1$  norm constraint by assuming sparsity in the temporal direction. Recently, in [20], both temporal and spatial sparsity are exploited to recover fMRI data. Here, CS is also utilized to gain high spatial resolution fMRI and method is named as High Spatial Resolution Compressed Sensing (HSPARSE) [20].

In [21],  $k$ - $t$  FASTER method is proposed that recovers a low rank signal via iterative hard thresholding of singular values of data matrix in the CS framework. In another work [22, 24], fMRI reconstruction is performed using low-rank plus sparse (LR+S) decomposition of fMRI signals. Here, an iterative framework is used that reconstructs the low rank and the sparse components of fMRI data separately.

In this paper, we introduce a novel offline fMRI reconstruction method. In fMRI, same brain volumes are scanned repeatedly over time in order to study brain’s function. This fact is used as an advantage in the proposed method via total variation based regularization [27] because scanning of the same brain volume over time brings similarity in the temporal direction. In addition, we impose conventional temporal sparsity in the proposed reconstruction framework. In other words, we impose two  $l^1$ -norm constraints. First  $l^1$ -norm sparsity is imposed on the voxel time series (temporal data) in the transformed domain and second  $l^1$  norm sparsity is imposed on the successive difference of the same temporal data. Hence, we name the proposed method as Double Temporal Sparsity based Reconstruction (DTSR) method.

We thoroughly evaluate the robustness and the feasibility of the proposed DTSR method both at subject and group levels of real fMRI data analysis. The performance of DTSR method has been preliminary evaluated using retrospective undersampling of the fully available fMRI dataset. We compare the performance of the proposed method with other offline methods such as Compressed Sensing with Wavelet domain Sparsity (CSWD) [19], HSPARSE [20],  $k$ - $t$  FASTER [21], and LR+S [22]. Results demonstrate that DTSR is able to improve BOLD sensitivity both at the individual and at the group level compared to other methods. Existing reconstruction methods produce greater artifact at high acceleration factors. The proposed DTSR reconstruction method increases temporal resolution without affecting the spatial resolution and can be used to provide accelerated high temporal resolution fMRI reconstruction with accurate detection of intrinsic brain’s Resting State Networks (RSNs). Please note that DTSR method has been developed for “resting state” fMRI.

Key contributions of this work are summarized as below:

- A double temporal-sparsity based reconstruction framework is proposed

for the robust reconstruction of undersampled fMRI data.

- An algorithm is designed to solve the proposed DTSR reconstruction approach using the state-of-the-art Alternating Direction Multiplier Method (ADMM).
- The performance of our proposed method is evaluated on fMRI dataset using both quantitative and qualitative analysis. Quantitative analysis in terms of Peak Signal-to-Noise Ratio (PSNR) and other metrics, and qualitative analysis in terms of reproducibility of brain RSNs demonstrate the robustness and efficacy of the proposed DTSR reconstruction method.

This paper is organized into five sections. In the Materials and Methods section, we discuss dataset description and some preliminary theory. In this section, we also present the proposed DTSR reconstruction method. We present experimental results on fMRI data in Section 3. We provide a thorough discussion of reconstruction results in section 4. In the end, conclusions are presented in section 5.

## 2. Materials and Methods

### 2.1. Dataset Description

The proposed DTSR method has been evaluated on the freely available Beijing\_Zang resting state fMRI dataset. This real fMRI dataset is a part of Neuroimaging Informatics Tools and Resources Clearinghouse (NITRC) 1000 functional connectomes project [28].

It consists of an acquisition of 33 axial interleaved ascending brain slices with a dimension of 64x64 at each time point with Repetition Time (TR) equal to 2 seconds. The fMRI brain data is collected over 225 time points. This dataset consists of 198 subjects' resting-state fMRI data, aged between 18 to 26 years of age and acquired while subjects' eyes were closed. For more details on this dataset, please refer to the website<sup>1</sup>. For this paper, data of first 20 subjects from the set of 198 Beijing\_Zang subjects has been downloaded from the 1000 functional connectomes project's online database.

### 2.2. Preliminaries

This subsection presents the CS-based fMRI reconstruction problem formulation. Consider a 4-D fMRI dataset  $\mathbb{R}^{n_x \times n_y \times n_z \times T}$ , where  $n_z$  denotes the number of brain slices with each slice of dimension  $n_x \times n_y$  and  $T$  denotes the number of time points. In fMRI, 3-D brain volumes (each volume is made up of  $n_z$  number of brain slices) are captured repeatedly over  $T$  number of time points.

Consider a Casorati matrix  $\mathbf{X} = [\mathbf{x}_1, \mathbf{x}_2, \dots, \mathbf{x}_T] \in \mathbb{R}^{n \times T}$  of any brain slice, where  $n = n_x \times n_y$  are the number of voxels in that brain slice and  $T$  denotes

---

<sup>1</sup>[http://fcon\\_1000.projects.nitrc.org/](http://fcon_1000.projects.nitrc.org/)

the total number of time points. Each column  $\mathbf{x}_t \in \mathbb{R}^n$  of  $\mathbf{X}$  represents the brain slice at the  $t^{\text{th}}$  time point. In accelerated fMRI, less amount of slice data is captured in the  $k$ -space in order to achieve quicker scanning of slices. This allows capturing of more brain volumes in a given time leading to higher temporal resolution. Consider  $\mathbf{Y}$  to be such a compressively sensed  $k$ -space data that can be represented as

$$\mathbf{Y} = \Phi \mathbf{F} \mathbf{X} + \xi, \quad (1)$$

where  $\mathbf{F}$  denotes the 2-D Fourier transform operator applied on the Casorati matrix  $\mathbf{X}$  for transforming this data to the  $k$ -space domain,  $\Phi$  is the sensing matrix that contains information about the partial measurements in the  $k$ -space domain, and  $\xi \in \mathbb{R}^{n \times T}$  denotes the measurement noise. Given a sensing matrix  $\Phi$ , the aim of any fMRI reconstruction method is to recover Casorati data matrix  $\mathbf{X}$  from partial Fourier measurements  $\mathbf{Y}$ . Reconstruction is done independently for all  $n_z$  brain slices.

The task of computing  $\mathbf{X}$  from  $\mathbf{Y}$  is an underdetermined inverse problem. It is not possible to solve (1) by computing the inverse because the sensing matrix  $\Phi$  in the forward equation is usually ill-conditioned due to large undersampling. Therefore, in general the problem needs to be regularized to find a solution. A relatively simple solution is a well known sparsity regularization [19].

Sparse recovery methods assume the desired signal to be sparse over some known *a priori* transform basis  $\Psi$  and hence,  $l^1$  norm in the corresponding domain is used as regularization to recover the signal.  $l^1$  norm is used as a surrogate for standard sparsity inducing  $l^0$  norm because regularization over  $l^0$  norm is a non-deterministic polynomial (NP) hard problem. Thus, using sparsity regularization, fMRI reconstruction problem can be formulated as

$$\hat{\mathbf{X}} = \arg \min_{\mathbf{X}} \|\mathbf{Y} - \Phi \mathbf{F} \mathbf{X}\|_F^2 + \lambda_1 \|\Psi \mathbf{X}\|_1, \quad (2)$$

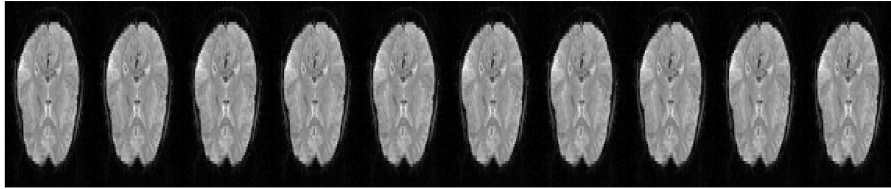
where  $\|\cdot\|_F^2$  denotes the Frobenius norm that is defined as  $\|\mathbf{Y} - \Phi \mathbf{F} \mathbf{X}\|_F^2 = \text{Tr}[(\mathbf{Y} - \Phi \mathbf{F} \mathbf{X})^T (\mathbf{Y} - \Phi \mathbf{F} \mathbf{X})]$ ,  $\Psi$  denotes the sparsifying transform basis,  $\|\cdot\|_1$  is the  $l^1$  norm, and  $\lambda_1$  is the regularization parameter that governs the sparsity on  $\mathbf{X}$  over the  $\Psi$  basis. The first term in (2) is the data fidelity term that minimizes the variance of noise  $\xi$ , while

$$\|\mathbf{A}\|_F^2 = \sum_{i=1}^n \sum_{j=1}^T a_{ij}^2 \quad \text{and} \quad \|\mathbf{A}\|_1 = \sum_{i=1}^n \sum_{j=1}^T |a_{ij}|. \quad (3)$$

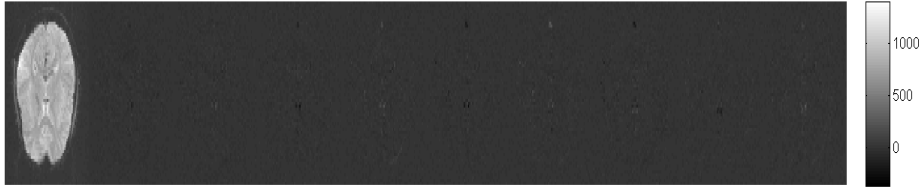
### 2.3. Proposed DTSR Method

Consider the Casorati matrix  $\mathbf{X}$  for any brain slice, where each column  $\mathbf{x}_t$  represents the vectorized brain slice captured at the  $t^{\text{th}}$  time point. Since a brain slice over adjacent time points may contain less amplitude changes, the difference of adjacent columns of this Casorati matrix exhibits strong sparsity. Fig.1 illustrates sparsity of the first difference between two consecutive axial brain slices. From this figure, it is reasonable to assume that the successive

difference of columns of Casorati matrix is sparse, i.e., the amplitude difference of slice at time point  $t$  and  $t-1$  is sparse. This form of difference sparsity is also known as total variation in the case of 1-D signal recovery [27]. We call this sparsity in the context of fMRI as total variation temporal sparsity because it exploits sparsity in the temporal direction. In addition to this, we also impose conventional temporal sparsity, i.e., the sparsity of the temporal data in some transform domain. In other words, we impose two  $l^1$ -norm constraints. First  $l^1$ -norm sparsity is imposed on the voxel time series (temporal data) in the transformed domain and second  $l^1$  norm sparsity is imposed on the successive difference of the same temporal data. Hence, we name the proposed method as Double Temporal Sparsity based Reconstruction (DTSR) method.



(a) Middle slice at 10 consecutive time points of one subject



(b) Difference images to show total variation temporal sparsity, where difference is computed over successive slices at  $t$  and  $t-1$  time points. First time point of brain slice is considered without differencing as shown.

Figure 1: Illustration of total variation temporal sparsity on middle slice of one subject’s fMRI data. Total variation temporal sparsity method arises due to repeated scanning of the same brain volume in fMRI to study brain’s function. Scanning of the same brain volume over time brings similarity in the temporal direction that can be utilized via total variation based regularization.

In the total variation temporal sparsity, the difference matrix of  $\mathbf{X}$  is assumed to be sparse. This difference matrix is formed by performing the first difference on the consecutive columns of  $\mathbf{X}$ . First differencing is performed from 2<sup>nd</sup>

column onwards. Thus, the DTSR objective function can be formulated as

$$\hat{\mathbf{X}} = \arg \min_{\mathbf{X}} \|\mathbf{Y} - \Phi \mathbf{F} \mathbf{X}\|_F^2 + \lambda_1 \|\Psi \mathbf{X}\|_1 + \lambda_2 \sum_{t=2}^T |\mathbf{x}_t - \mathbf{x}_{t-1}|, \quad (4)$$

where  $\lambda_1$  and  $\lambda_2$  are non-negative regularization parameters. Since second regularization term in (4) is non-differentiable, it is not easy to solve DTSR in this formulation. Thus, (4) is reformulated below with matrix version that provides efficient solution to this problem.

$$\hat{\mathbf{X}} = \arg \min_{\mathbf{X}} \|\mathbf{Y} - \Phi \mathbf{F} \mathbf{X}\|_F^2 + \lambda_1 \|\Psi \mathbf{X}\|_1 + \lambda_2 \|\mathbf{X} \mathbf{D}\|_1. \quad (5)$$

Here,  $\mathbf{D}$  performs first order differencing on the successive columns of the given matrix  $\mathbf{X}$  and is defined as:

$$\mathbf{D} = \begin{bmatrix} -1 & 1 & 0 & \cdot & \cdot & 0 & 0 \\ 0 & -1 & 1 & 0 & \cdot & \cdot & 0 \\ 0 & 0 & -1 & 1 & 0 & \cdot & \cdot \\ 0 & 0 & \cdot & \cdot & \cdot & \cdot & \cdot \\ \cdot & \cdot & \cdot & \cdot & \cdot & \cdot & 0 \\ 0 & \cdot & \cdot & \cdot & 0 & -1 & 1 \\ 0 & 0 & \cdot & 0 & 0 & 0 & -1 \end{bmatrix}.$$

The total variation temporal sparsity is illustrated on Beijing\_Zang dataset in Fig.2a and Fig.2b that plot sorted values of  $\mathbf{X}$  and  $\mathbf{X} \mathbf{D}$ , respectively. All 33 slices of one randomly selected subject's data is used in these figures. This figure indicates that the sparsity assumption on  $\mathbf{X} \mathbf{D}$  is reasonably valid.

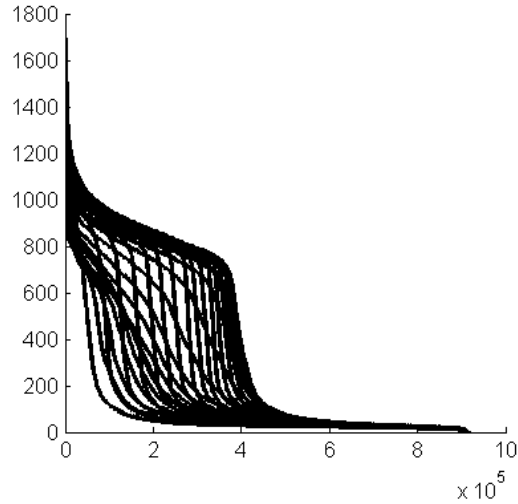
### 2.3.1. Algorithm Design

In this subsection, an algorithm is designed to solve (5) using the alternating direction multiplier method (ADMM) [29]. ADMM is suitable for constrained optimization problems and is being used extensively since past few years [30, 31, 32, 33, 34, 35]. This technique facilitates solution by decomposing the original objective function into multiple objective functions that are easy to solve.

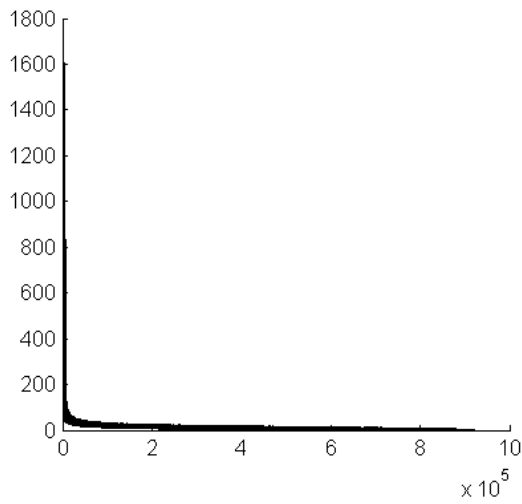
Following [29], two auxiliary matrices  $\mathbf{W} \in \mathbb{R}^{n \times T}$  and  $\mathbf{Z} \in \mathbb{R}^{n \times T}$  are introduced in (5) as

$$\hat{\mathbf{X}} = \arg \min_{\mathbf{X}} \|\mathbf{Y} - \Phi \mathbf{F} \mathbf{X}\|_F^2 + \lambda_1 \|\mathbf{W}\|_1 + \lambda_2 \|\mathbf{Z}\|_1 \quad (6)$$

*s.t.*  $\mathbf{W} = \Psi \mathbf{X}, \mathbf{Z} = \mathbf{X} \mathbf{D}.$



(a) Decay of coefficients of  $\mathbf{X}$



(b) Decay of coefficients of  $\mathbf{XD}$

Figure 2: Illustration of sparsity of  $\mathbf{X}$  and  $\mathbf{XD}$ , where  $\mathbf{X}$  represents a brain slice stacked over all time points and  $\mathbf{D}$  performs first differencing on the successive columns of the given matrix  $\mathbf{X}$ , or in other words performs total variation temporal sparsity. Fig.2a and Fig.2b plot sorted coefficients of  $\mathbf{X}$  and  $\mathbf{XD}$  corresponding to a Beijing\_Zang dataset. Black lines correspond to sorted decaying coefficients of multiple a)  $\mathbf{X}$ ; and b)  $\mathbf{XD}$  matrices corresponding to all 33 slices of one random subject. This figure indicates that the Fig.2b has more sparse coefficients compare to Fig.2a. In other words, we observe  $\mathbf{XD}$  to be sparser than  $\mathbf{X}$  on Beijing\_Zang fMRI dataset.

In addition to this, constraints with equality are added for each of the auxiliary matrices. Thus, the new objective function is written as:

$$\begin{aligned} \arg \min_{\mathbf{X}, \mathbf{Z}, \mathbf{W}} & \|\mathbf{Y} - \Phi \mathbf{F} \mathbf{X}\|_F^2 + \lambda_1 \|\mathbf{W}\|_1 + \lambda_2 \|\mathbf{Z}\|_1 + \\ & \frac{\eta_1}{2} \|\mathbf{W} - \Psi \mathbf{X} - \mathbf{B}_1\|_F^2 + \frac{\eta_2}{2} \|\mathbf{Z} - \mathbf{X} \mathbf{D} - \mathbf{B}_2\|_F^2, \end{aligned} \quad (7)$$

where  $\eta_1$  and  $\eta_2$  are penalty parameters and,  $\mathbf{B}_1$  and  $\mathbf{B}_2$  are the Lagrange multipliers used to enforce equality between the original and auxiliary matrices.

ADMM updates variables  $\mathbf{W}$ ,  $\mathbf{Z}$ , and  $\mathbf{X}$  alternately in the above defined augmented Lagrangian function. The minimization over one variable in an iteration assumes the other two variables to be fixed. Therefore, the above function can be alternately optimized over each variable separately. This allows splitting of (7) into different subproblems with three new objective functions stated as below:

$$P1: \arg \min_{\mathbf{W}} \lambda_1 \|\mathbf{W}\|_1 + \frac{\eta_1}{2} \|\mathbf{W} - \Psi \mathbf{X}^{j-1} - \mathbf{B}_1^{j-1}\|_F^2, \quad (8)$$

$$P2: \arg \min_{\mathbf{Z}} \lambda_2 \|\mathbf{Z}\|_1 + \frac{\eta_2}{2} \|\mathbf{Z} - \mathbf{X}^{j-1} \mathbf{D} - \mathbf{B}_2^{j-1}\|_F^2, \quad (9)$$

$$\begin{aligned} P3: \arg \min_{\mathbf{X}} & \|\mathbf{Y} - \Phi \mathbf{F} \mathbf{X}\|_F^2 + \frac{\eta_1}{2} \|\mathbf{W}^j - \Psi \mathbf{X} - \mathbf{B}_1^{j-1}\|_F^2 + \\ & \frac{\eta_2}{2} \|\mathbf{Z}^j - \mathbf{X} \mathbf{D} - \mathbf{B}_2^{j-1}\|_F^2, \end{aligned} \quad (10)$$

where  $j$  is the iteration number.  $P1$  and  $P2$  subproblems minimize objective functions over  $\mathbf{W}$  and  $\mathbf{Z}$ , respectively, with fixed  $\mathbf{X}$ .  $P3$  minimizes the objective function over  $\mathbf{X}$  with fixed  $\mathbf{W}$  and  $\mathbf{Z}$ . Above three subproblems are solved iteratively along with the update of Lagrange multipliers  $\mathbf{B}_1$  and  $\mathbf{B}_2$ . The complete algorithm is summarized in Algorithm 1, while the solution of each subproblem is explained in the next few subsections.

### 2.3.2. $P1$ and $P2$ Subproblems

The first two subproblems are  $l^1$  minimization problems. For any  $l^1$  minimization problem such as

$$\min_{\mathbf{P}} \alpha \|\mathbf{P}\|_1 + \frac{\beta}{2} \|\mathbf{P} - \mathbf{Q}\|_F^2, \quad (11)$$

where  $\mathbf{P}, \mathbf{Q} \in \mathbf{R}^{n \times T}$  and  $\alpha, \beta > 0$ , the solution is [25]

$$\mathbf{P} = \text{Soft}(\mathbf{Q}, 2\frac{\alpha}{\beta} \mathbf{A}), \quad (12)$$

---

**Algorithm 1** Pseudo code of the proposed DTSR method
 

---

- 1: Initialize  $\lambda_1, \lambda_2, \eta_1, \eta_2, \mathbf{B}_1^0, \mathbf{B}_2^0, \mathbf{X}^0, j=1$
- 2: **while** convergence criteria not met **do**
- 3:   *P1*-subproblem

$$\mathbf{W}^j = \arg \min_{\mathbf{W}} \lambda_1 \|\mathbf{W}\|_1 + \frac{\eta_1}{2} \left\| \mathbf{W} - \Psi \mathbf{X}^{j-1} - \mathbf{B}_1^{j-1} \right\|_F^2.$$

- 4:   *P2*-subproblem

$$\mathbf{Z}^j = \arg \min_{\mathbf{Z}} \lambda_2 \|\mathbf{Z}\|_1 + \frac{\eta_2}{2} \left\| \mathbf{Z} - \mathbf{X}^{j-1} \mathbf{D} - \mathbf{B}_2^{j-1} \right\|_F^2.$$

- 5:   *P3*-subproblem

$$\begin{aligned} \mathbf{X}^j = \arg \min_{\mathbf{X}} & \|\mathbf{Y} - \Phi \mathbf{F} \mathbf{X}\|_F^2 + \frac{\eta_1}{2} \left\| \mathbf{W}^j - \Psi \mathbf{X} - \mathbf{B}_1^{j-1} \right\|_F^2 \\ & + \frac{\eta_2}{2} \left\| \mathbf{Z}^j - \mathbf{X} \mathbf{D} - \mathbf{B}_2^{j-1} \right\|_F^2. \end{aligned}$$

- 6:   Lagrange multipliers update

$$\begin{aligned} \mathbf{B}_1^j &= \mathbf{B}_1^{j-1} + \Psi \mathbf{X}^j - \mathbf{W}^j. \\ \mathbf{B}_2^j &= \mathbf{B}_2^{j-1} + \mathbf{X}^j \mathbf{D} - \mathbf{Z}^j. \end{aligned}$$

- 7:    $j=j+1$
  - 8: **end while**
-

where  $\mathbf{A}$  is a matrix containing all ones and  $\mathbf{Q}$  on the right hand side in the above equation is an initial estimate of  $\mathbf{P}$ . The definition of ‘*Soft*’ is

$$Soft(\mathbf{Q}, \nu \mathbf{A}) = sgn(\mathbf{Q}) \otimes max\{0, |\mathbf{Q}| - \nu \mathbf{A}\}, \quad (13)$$

where  $\nu = \frac{\alpha}{\beta}$ ,  $\otimes$  denotes the element-wise product, and  $|\mathbf{Q}|$  denotes a matrix with absolute values of  $\mathbf{Q}$ .  $\mathbf{A}$  in the above equation ensures soft thresholding on all elements of  $\mathbf{Q}$ . For the nonzero elements of  $\mathbf{Q}$ ,  $sgn(\mathbf{Q}) = \mathbf{Q}./|\mathbf{Q}|$ , otherwise  $sgn(\mathbf{Q}) = 0$ .

Hence, the closed form solution of  $\mathbf{W}$  at the iteration number  $j$  in the  $P1$ -subproblem is

$$\mathbf{W}^j = Soft((\Psi \mathbf{X}^{j-1} + \mathbf{B}_1^{j-1}), 2 \frac{\lambda_1}{\eta_1} \mathbf{A}). \quad (14)$$

Once  $\mathbf{W}$  at iteration  $j$  is estimated from the subproblem  $P1$ , the next step is to estimate  $\mathbf{Z}$  from the subproblem  $P2$ . Using  $\mathbf{X}^{j-1}$  and  $\mathbf{B}_2^{j-1}$  from the previous iteration,  $\mathbf{Z}^j$  can be obtained via a closed form as

$$\mathbf{Z}^j = Soft((\mathbf{X}^{j-1} D + \mathbf{B}_2^{j-1}), 2 \frac{\lambda_2}{\eta_2} \mathbf{A}). \quad (15)$$

### 2.3.3. *P3 Subproblem*

This subproblem is quadratic. It can be efficiently solved using the conjugate gradient algorithm. We used the line search conjugate gradient algorithm as used in [35]. This is an iterative method where, first, a descent direction is decided based on the minimization of objective function. Next, a step size is computed that determines how far the unknown variable of interest should move along the descent direction. Unlike a fixed step size in the normal gradient descent, this method performs a line search in order to find the best step size. In general, it has been observed that for convex quadratic objective functions, the line search conjugate gradient method achieves a finite convergence.

### 2.3.4. *Update of Lagrange Multiplier Variables*

Last step is the update of Lagrange multipliers that is explained in Algorithm 1. Lagrange multipliers help in achieving convergence in the subsequent iterations. In this algorithm, convergence is checked either by comparing convergence of the objective function in (4) with a threshold or with the maximum number of iterations reached.

## 3. Results

### 3.1. *Implementation Details*

#### 3.1.1. *Temporal Sparsity Domain*

In general, sparsity is imposed in the transform domain  $\Psi$  as shown in (2) and (4). Recently, in our previous work [25], we observed that fMRI data is more sparse in the temporal Fourier domain, i.e., in the Fourier domain of

every voxel’s time series. Hence, the matrix resulting by computing the Fourier transform of  $\mathbf{X}$  along every row leads to a temporal Fourier transformed matrix that is sparse. In order to demonstrate this, we plot the sorted temporal Fourier transformed coefficients of matrix  $\mathbf{X}$  corresponding to the middle slice of one subject of Beijing\_Zang data (Refer to Fig.3).

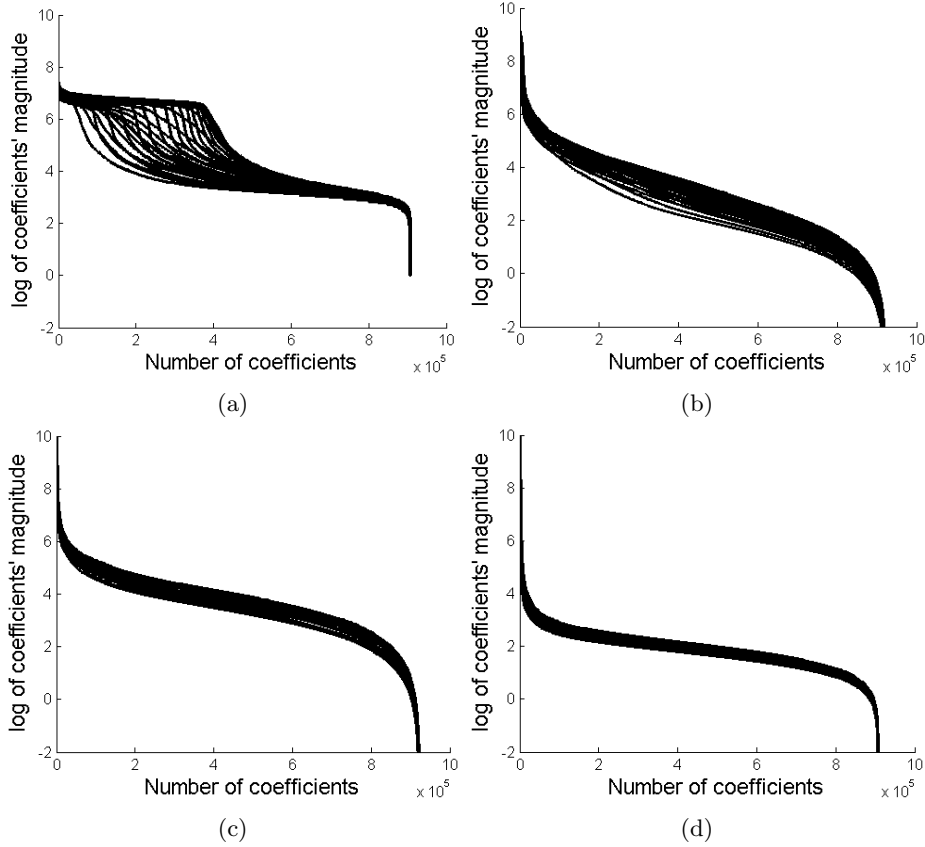


Figure 3: Illustration of increased sparsity of Beijing\_Zang fMRI data in the temporal Fourier Transform domain. One subject’s sorted log magnitude values of coefficients of matrix  $\mathbf{X}$  obtained using: (a) no transform; (b) 3-level dB4 wavelet in spatial direction; (c) 2-D Discrete Cosine Transform in spatial directions; (d) 1-D Discrete Fourier Transform along the rows of  $\mathbf{X}$ .

From these figures, we observe that fMRI data is sparser in the temporal frequency domain. Hence, in (4), we consider  $\Psi$  as the corresponding temporal Fourier domain sparsifying matrix, i.e., it computes the Fourier transform along every row of  $\mathbf{X}$ .

### 3.1.2. Retrospective Undersampling

In this paper, undersampled  $k-t$  space data  $\mathbf{Y}$  is acquired by retrospective undersampling of the Fourier transform of the fully available data. Radial sampling patterns are used to undersample available  $k$ -space data as used in [36, 24, 25]. These patterns represent different sampling masks used for one brain slice of size  $n_x \times n_y$  at one time point with zeros at non-sampled locations and ones at sampled locations. Sensing matrix  $\Phi$  in (4) is constructed by stacking sampling masks of all  $T$  time points.

### 3.1.3. Regularization Parameters

The proposed DTSR method requires seven parameters  $\lambda_1, \lambda_2, \eta_1, \eta_2, \mathbf{B}_1^0, \mathbf{B}_2^0$ , and  $\mathbf{X}^0$  to be initialized as shown in Algorithm 1.  $\eta_1$  and  $\eta_2$  are initialized as  $10^{-2}$ . Lagrange multipliers  $\mathbf{B}_1^0$  and  $\mathbf{B}_2^0$  are initialized to matrices containing all one's. We used  $L$ -curve method to initialize  $\lambda_1$  and  $\lambda_2$  [37] based on the maximization of peak signal-to-noise ratio (PSNR) compared to the ground truth (fully available dataset).  $L$ -curve method is an iterative approach of finding regularization parameters. In this method, one parameter value is fixed initially and the optimal value of other parameters is decided based on any objective criteria. For example, we are trying to maximize the PSNR and hence, this is our objective function. Next, the first parameter is fixed and the objective function is optimized over the second parameter. We empirically tested  $\lambda_1$  and  $\lambda_2$  in the range of  $(10^{-4}, 10^{-3} \dots 10^3, 10^4)$  and arrived at the following values:  $\lambda_1 = \lambda_2 = 0.5$ . The fMRI data matrix  $\mathbf{X}^0$  in subproblem  $P1$  is initialized using the crude initial estimate obtained via direct inverse Fourier transform (IFT). Direct IFT method computes IFT of given  $k-t$  space data  $\mathbf{Y}$  as shown below:

$$\mathbf{X}^0 = IFT(\mathbf{Y}). \quad (16)$$

## 3.2. Related Reconstruction Methods

We compare results of the proposed DTSR method with other offline fMRI reconstruction methods including CSWD [19], HSPARSE [20],  $k-t$  FASTER [21], and LR+S [22]. Below we present brief overview of each of the reconstruction methods implemented. We also provide regularization parameter values used in the simulation of these methods.

### 3.2.1. CS with Wavelet Domain Sparsity (CSWD) [19]

In this method, compressive sensing based reconstruction of fMRI data is carried out assuming the fMRI data to be spatially sparse in the wavelet domain [19]. Hence, fMRI reconstruction is done by using the optimization framework as explained in (2). Here,  $\Psi$  is a wavelet matrix operator. We used Daubechies orthogonal wavelet 'db4' (filter lengths 8) with 3-level decomposition as used in [19]. We used non-linear conjugate gradient method to solve CSWD [38]. We used the default value of  $\lambda_1 = 0.1$  as specified in this method.

### 3.2.2. HSPARSE Method [20]

The HSPARSE method reconstructs fMRI data assuming data matrix  $\mathbf{X}$  to be sparse in both the temporal and spatial domains. This method is implemented by solving the below optimization problem [20]:

$$\hat{\mathbf{X}} = \arg \min_{\mathbf{X}} \|\mathbf{Y} - \Phi \mathbf{F} \mathbf{X}\|_F^2 + \lambda_3 \|\Psi_t \mathbf{X}\|_1 + \lambda_4 \|\Psi_s \mathbf{X}\|_1, \quad (17)$$

where  $\lambda_3$  and  $\lambda_4$  are regularization parameters and,  $\Psi_t$  and  $\Psi_s$  are the temporal and spatial domain sparsifying basis, respectively. We chose discrete cosine transform (DCT) for both the temporal and the spatial sparsity as used in [20] and  $\lambda_3=0.5$  and  $\lambda_4=0.1$  in (17) for simulation. We used the non-linear conjugate gradient method to solve HSPARSE [38].

### 3.2.3. $k$ -t FASTER Method [21]

$k$ -t FASTER method reconstructs fMRI data assuming data matrix  $\mathbf{X}$  to be low rank. This method is implemented by solving the below optimization problem [21]:

$$\hat{\mathbf{X}} = \arg \min_{\mathbf{X}} \|\mathbf{Y} - \Phi \mathbf{F} \mathbf{X}\|_F^2 \quad s.t \quad rank(\mathbf{X}) = r, \quad (18)$$

where  $r$  is the pre-defined rank of  $\mathbf{X}$ . In  $k$ -t FASTER [21], hard thresholding is applied on the singular values of data matrix  $\mathbf{X}$  as explained below. First, singular value decomposition (SVD) of an initial crude estimate of matrix  $\mathbf{X}^0$  is computed

$$\mathbf{X}^0 = \mathbf{U} \mathbf{S} \mathbf{V}^T. \quad (19)$$

Next, hard thresholding is applied on the singular values contained in  $\mathbf{S}$  as

$$\hat{s}_i = \begin{cases} |s_i| - \mu & i \leq r \\ 0 & i > r \end{cases} \quad (20)$$

where  $\mu$  is a constant,  $s_i$  is the  $i^{th}$  singular value of  $\mathbf{S}$ , and  $\hat{s}_i$  is updated singular value after hard thresholding.

The value of constant  $\mu$  is chosen to be 0.5 as used in [21]. In simulation, rank  $r$  is considered to be equal to the number of time frames. This value provided least normalized mean square error (NMSE) between the reconstructed and the original fMRI data considered in this work.

### 3.2.4. Low Rank plus Sparse (LR+S) Method [22]

This method reconstructs fMRI data using low rank and sparse matrix decomposition and hence, is solved using the following optimization framework:

$$\hat{\mathbf{L}}, \hat{\mathbf{S}} = \arg \min_{\mathbf{L}, \mathbf{S}} \|\mathbf{Y} - \Phi \mathbf{F} (\mathbf{L} + \mathbf{S})\|_F^2 + \lambda_5 \|\mathbf{L}\|_* + \lambda_6 \|\mathbf{S}\|_1, \quad (21)$$

where  $\lambda_5$  and  $\lambda_6$  are the regularization parameters. The fMRI data matrix  $\mathbf{X}$  is reconstructed as:

$$\hat{\mathbf{X}} = \hat{\mathbf{L}} + \hat{\mathbf{S}}. \quad (22)$$

We empirically selected  $\lambda_5 = 300$  and  $\lambda_6 = 0.5$  that provided us the minimum NMSE.

The default number of iterations used in the non-linear conjugate algorithm in CSWD [19] and HSPARSE [20] is 20 [38]. Hence, for other reconstruction methods including DTSR, we have set the maximum number of iterations (required in optimization) to 20 and the convergence threshold of objective function to  $10^{-5}$ . Since LR+S [22] method converges in more number of iterations, we predefined the maximum number of iterations to 100 for this method.

### 3.3. Quantitative Analysis

In this section, we compare results of the proposed DTSR against the existing CS-based fMRI reconstruction methods. The Normalized Mean Square Error (NMSE), PSNR, and Structural Similarity Index (SSIM) are used as reconstruction quality assessment metrics in this paper.

NMSE and PSNR are two well known reconstruction quality assessment metrics. Given a reference brain slice  $\mathbf{x}_t$  at time point  $t$  and its reconstructed estimate  $\hat{\mathbf{x}}_t$  ( $t^{th}$  column of  $\hat{\mathbf{X}}$ ), NMSE is calculated as

$$\text{NMSE} = \|\mathbf{x}_t - \hat{\mathbf{x}}_t\|_2 / \|\mathbf{x}_t\|_2, \quad (23)$$

where  $\|\cdot\|_2$  denotes  $l^2$  norm. Similarly PSNR is calculated as

$$\text{PSNR} = 20 \log_{10} \frac{255}{\frac{1}{n_x n_y} \|\mathbf{x}_t - \hat{\mathbf{x}}_t\|_2}, \quad (24)$$

where  $n_x \times n_y$  denotes the size of brain slices. In this work, one slice is being reconstructed simultaneously over all time points. Hence, NMSE and PSNR are calculated using (23) and (24) for  $T$  number of time points for a given slice and are subsequently time-averaged. In the following text, NMSE and PSNR signify average NMSE and average PSNR. SSIM is also used to measure the reconstruction quality by measuring luminous, contrast, and structural similarity between the reconstructed and original images [39]. It is known to be a better metric than NMSE and PSNR [39]. For original slice  $\mathbf{x}_t$  and its reconstructed estimate  $\hat{\mathbf{x}}_t$  at time point  $t$ , SSIM is defined as [39]:

$$\text{SSIM}(\mathbf{x}_t, \hat{\mathbf{x}}_t) = l(\mathbf{x}_t, \hat{\mathbf{x}}_t) c(\mathbf{x}_t, \hat{\mathbf{x}}_t) s(\mathbf{x}_t, \hat{\mathbf{x}}_t), \quad (25)$$

where luminous  $l(\mathbf{x}_t, \hat{\mathbf{x}}_t)$ , contrast  $c(\mathbf{x}_t, \hat{\mathbf{x}}_t)$ , and structural  $s(\mathbf{x}_t, \hat{\mathbf{x}}_t)$  components are defined as:

$$\begin{aligned} l(\mathbf{x}_t, \hat{\mathbf{x}}_t) &= \frac{2\mu_{\mathbf{x}_t} \mu_{\hat{\mathbf{x}}_t} + C_1}{\mu_{\mathbf{x}_t}^2 + \mu_{\hat{\mathbf{x}}_t}^2 + C_1} \\ c(\mathbf{x}_t, \hat{\mathbf{x}}_t) &= \frac{2\sigma_{\mathbf{x}_t} \sigma_{\hat{\mathbf{x}}_t} + C_2}{\sigma_{\mathbf{x}_t}^2 + \sigma_{\hat{\mathbf{x}}_t}^2 + C_2} \\ s(\mathbf{x}_t, \hat{\mathbf{x}}_t) &= \frac{\sigma_{\mathbf{x}_t \hat{\mathbf{x}}_t} + C_3}{\sigma_{\mathbf{x}_t} \sigma_{\hat{\mathbf{x}}_t} + C_3}, \end{aligned} \quad (26)$$

where  $\mu_{\mathbf{x}_t}$  and  $\mu_{\hat{\mathbf{x}}_t}$  denote the mean of the original and reconstructed slices respectively,  $\sigma_{\mathbf{x}_t}$  and  $\sigma_{\hat{\mathbf{x}}_t}$  represent their standard deviations, and  $\sigma_{\mathbf{x}_t\hat{\mathbf{x}}_t}$  denotes the covariance between these two slices.  $C_1$ ,  $C_2$  and  $C_3$  are constants, chosen to avoid zero in the denominator. SSIM is generally computed on  $8 \times 8$  patches of the original and reconstructed images. For this patch size  $C_1$ ,  $C_2$ , and  $C_3$  are defined as  $(K_1 2^8)^2$ ,  $(K_2 2^8)^2$ ,  $\frac{(K_3 2^8)^2}{2}$ , respectively, with  $K_1 = 0.01$  and  $K_2 = 0.03$  [39]. The final score over the entire slice size is obtained by averaging and is denoted as mean SSIM. Value of SSIM is bounded between  $(-1, 1)$  with value 1 signifying  $\mathbf{x}_t = \hat{\mathbf{x}}_t$ .

Reconstructed (average) NMSE, (average) PSNR, and (average) SSIM results over all 33 slices averaged over all subjects are presented in Table 1 and 2. Results are tabulated at 6, 12, and 24 number of radial sampling lines. From these results, we observe that the proposed DTSR performs consistently better than the existing reconstruction methods. This is to note that the proposed DTSR method assumes double sparsity in the temporal domain. Hence, it yields better results compared to the existing methods and also reconstructs fMRI data quite efficiently at lower number of radial sampling lines. Of note, we also tested performance of DTSR method with shorter TR dataset and obtained similar consistent results. This shows that the proposed method also works on shorter TR dataset.

Table 1: Mean reconstruction results with different methods on real fMRI dataset<sup>a</sup>

	NMSE			PSNR		
Method	6 lines	12 lines	24 lines	6 lines	12 lines	24 lines
CSWD [19]	0.2478	0.1689	0.1247	5.78	8.45	11.59
HSPARSE [20]	0.1752	0.0785	0.0551	7.989	13.895	18.014
k-t FASTER [21]	0.2476	0.1697	0.1178	4.878	8.412	11.758
LR+S [22]	0.1857	0.0783	0.0604	9.012	13.846	19.781
Proposed DTSR	<b>0.0541</b>	<b>0.0351</b>	<b>0.031</b>	<b>19.14</b>	<b>21.76</b>	<b>22.01</b>

<sup>a</sup> Dataset- Beijing\_Zang resting state fMRI data, results are averaged over all slices, over all time points, and over all subjects.

We observe that NMSE and PSNR are consistently very high at all acceleration factors considered including lower acceleration factors. This implies that we can reconstruct fMRI data by sampling much lesser measurements in  $k-t$  space with the proposed DTSR method compared to the other methods. Hence, higher acceleration is possible with the DTSR method that in turn will decrease the fMRI acquisition time.

Fig.4 presents (average) PSNR results over all slices of Beijing\_Zang fMRI data of 5 subjects. Six radial lines are used for undersampling the  $k$ -space data (12.856 acceleration factor). These results indicate that the proposed DTSR method is robust to subject variability and that the results are reproducible across subjects.

Table 2: Mean SSIM performance on Beijing\_Zang fMRI dataset<sup>a</sup> reconstructed with different methods

	<b>SSIM</b>		
<b>Method</b>	<b>6 lines</b>	<b>12 lines</b>	<b>24 lines</b>
CSWD [19]	0.3589	0.6012	0.7124
HSPARSE [20]	0.5356	0.8132	0.887
k-t FASTER [21]	0.3785	0.6785	0.7586
LR+S [22]	0.5284	0.7969	0.9045
Proposed DTSR	<b>0.9209</b>	<b>0.9541</b>	<b>0.9785</b>

<sup>a</sup> Dataset- Beijing\_Zang resting state fMRI data, results are averaged over all slices, over all time points, and over all subjects.

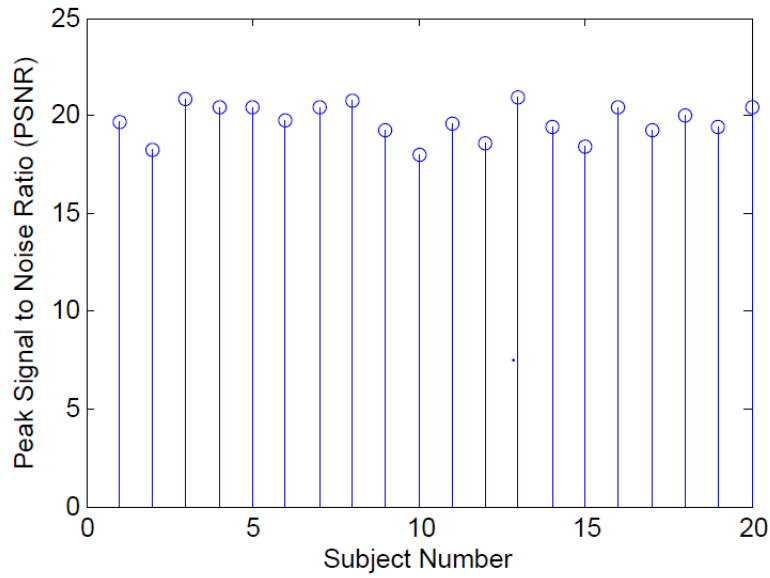


Figure 4: Illustration of reconstruction performance (in terms of average PSNR) over different subjects of Beijing\_Zang data

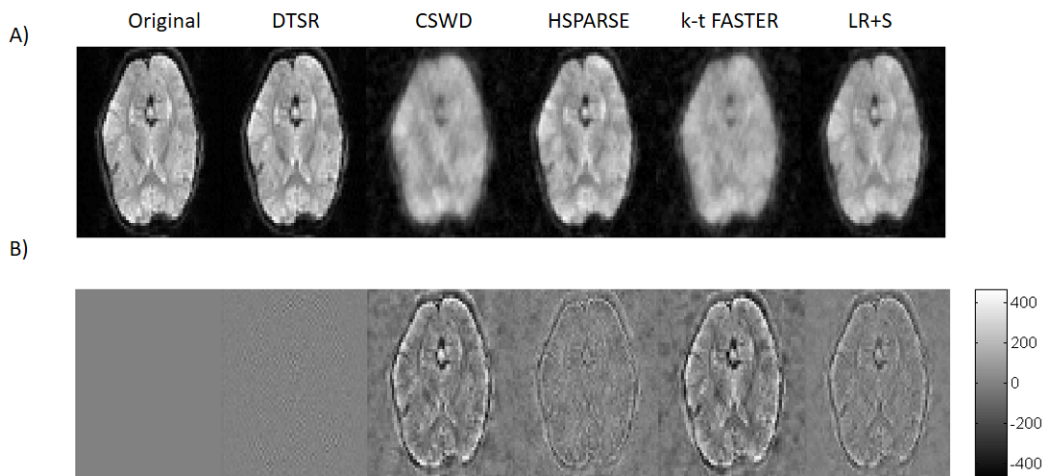


Figure 5: Reconstructed middle slice (slice no.16 (total slices = 33)) using different reconstruction methods with 6 radial lines. Left to right: original; proposed DTSR; CSWD; HSPARSE, k-t FASTER; LR+S. A) The reconstructed middle slice obtained using different methods on the Beijing\_Zang fMRI data of one randomly selected subject and at one random time point. B) Difference images (Ground truth Reconstructed) corresponding to the original slice presented in column one of subfigure-(A)

Furthermore, to visually compare the data reconstructed using different methods, we present reconstructed middle slice (slice no.16 (total slices = 33)) in Fig.5 on one random subject and at one random time point using six radial lines. From Fig.5, we observe that the reconstruction quality with the proposed DTSR method is superior compared to the existing methods.

### 3.4. Qualitative Analysis

In this section, we compare and evaluate the reproducibility of brain RSNs constructed using the proposed DTSR based reconstruction fMRI data and using the fully available whole brain resting fMRI dataset. Spatial Independent Component Analysis (ICA) of the reconstructed fMRI data and the original fully available fMRI dataset is performed via GIFT toolbox<sup>2</sup>. ICA is a data driven method that has been widely used in resting state fMRI to recover the set of spatially independent brain RSNs [40, 41, 42, 43, 44].

#### 3.4.1. Data Preprocessing

fMRI data suffers from low SNR and hence, needs to be preprocessed before analysis. Preprocessing is performed using SPM12 (Statistical Parametric Mapping)<sup>3</sup> and Matlab. The fMRI brain volumes are slice-time corrected using the

<sup>2</sup><https://www.nitrc.org/projects/gift>

<sup>3</sup><http://www.fil.ion.ucl.ac.uk/spm/software/spm12/>

middle slice (16, total slices=33) as a reference, realigned to the mean image, spatially normalized onto the Montreal Neurological Institute (MNI) space (3-mm isotropic voxels), and are spatially smoothed with a Gaussian kernel (Full Width Half Maximum (FWHM)=4 mm).

### 3.4.2. The ICA Model

For the sake of completeness, ICA model as used in fMRI is briefly discussed in this subsection. Consider matrix  $\mathbf{S} \in \mathbb{R}^{T \times V}$ , where  $T$  is the number of time points and  $V$  is the total number of voxels. After ICA,  $\mathbf{S}$  can be expressed as:

$$\mathbf{S} = \mathbf{M}\mathbf{N}, \quad (27)$$

where  $\mathbf{M}$  is the  $T \times C$  mixing matrix and  $\mathbf{N}$  is the  $C \times V$  source matrix.  $C$  is the total number of spatially independent component. Each row of source matrix  $\mathbf{N}$  represents one spatially independent component and the corresponding column of the mixing matrix  $\mathbf{M}$  represents time course of that independent component. The goal of spatial ICA is to model fMRI data as a mixture of maximally independent spatial components.

In this paper, the InfomaxICA algorithm [45] is used to obtain ICA components and the corresponding time courses. It is one of the most popular ICA algorithms that is used in fMRI data analysis [46]. The number of spatially independent components  $C$  is predefined to 100 in accordance with the previous studies [41, 42, 43, 44]. High number of components facilitate good segregation of cortical and subcortical brain functional networks [41].

To identify brain RSNs among 100 spatially independent components, spatial distribution of each component can be identified by spatial overlapping with the available template images of brain RSNs. We identified 51 ICs from the mean maps of all 20 fully available fMRI subjects after removing the artifact components. These ICs can be broadly categorized into 10 RSNs: 1. Visual Network (VN), 2. SomatoMotor Network (SMN), 3. Limbic Network (LN), 4. Dorsal Attention Network (DAN), 5. Ventral Attention Network (VAN), 6. Default Mode Network (DMN), 7. Frontoparietal Network (FPN), 8. Temporal + Frontal Network (TFN), 9. Subcortical Network (SCN), and 10. Cerebellar Network (CN).

On the fMRI data reconstructed using the proposed DTSR method, we identified 56 ICs from the mean maps of reconstructed fMRI data of all 20 subjects. We manually arranged these ICs into various RSNs stated above. The spatial maps of some RSNs discovered by the fully available Beijing\_Zang data and the DTSR reconstructed data are shown in Fig.6 to Fig.7. Left part of each figure represents networks identified using the fully available data and the right part represents networks identified using the DTSR reconstructed data. It is clear that spatial activation maps of RSNs obtained from the reconstructed data overlap significantly with the RSNs of the fully available fMRI data. From now onwards, ICs of DTSR reconstructed data will be mentioned as simply DTSR ICs (DTSR-ICs) and ICs of fully sampled original data will be mentioned as raw ICs (RICs). It is noticed that DTSR-IC maps are more enhanced compared

to the RIC maps. This is perhaps due to denoising inherent within the CS reconstruction framework.

**Table 3:** ICA time courses obtained with fully sampled original Beijing\_Zang data and DTSR reconstructed data are shown in Fig.6-7. An independent sample  $t$ -test is carried to test the hypothesis if there is any statistically significant difference between the ICA components of fully sampled original data and those of DTSR based reconstructed data. The test failed at the significance level of  $p < 0.05$  signifying that these are no statistical differences in these ICA components.

Original data	DTSR data	Correlation
IC 74	IC 90	<b>0.969</b>
IC 36	IC 5	<b>0.884</b>
IC 54	IC 63	<b>0.754</b>
IC 97	IC 97	<b>0.962</b>
IC 44	IC 52	<b>0.944</b>
IC 33	IC 25	<b>0.735</b>

In addition, we also evaluated the relationship between the ICA components using paired correlation. We present these results in Table 3, column 3. The corresponding ICA components of the original Beijing\_Zang data and using the DTSR method based reconstructed data are highly correlated. This result is inline with visual comparison results on ICA maps shown in Fig. 6 and 7.

From Fig.5, we note that existing methods result in greater artifact compared to both the original Beijing\_Zang data and the data obtained using the DTSR method. Further, we evaluated their performance in terms of reproducibility of ICA activation maps. One random activation map obtained using existing methods is presented in Fig.8. From this figure, we observe that false maps are being detected with CSWD, HSPARSE,  $k$ - $t$  FASTER, and LR+S methods that can lead to misleading findings based on RSNs.

This is to note that the DTSR-ICs of the reconstructed dataset matched with the RICs of fully sampled original data. Further, three additional ICs are observed with the DTSR reconstructed data that are not visible with the IC analysis of the original data. Fig.9 shows that these three ICs are actually the part of DMN and SMN. This shows that the data reconstructed using the proposed DTSR method has better RSN construction ability compared to the raw (original) data. This is to note that every RSN is observed to be present in all 20 subjects. This observation is in order because DTSR method denoises the data during reconstruction and hence, provides better network construction. However, in order to demonstrate the reproducibility of RSNs within and across subjects, we will test DTSR-ICs on several runs from individual subjects in the future work.

#### 4. Discussion

This study proposes DTSR method that provides accelerated fMRI data reconstruction by imposing double temporal sparsity. Proposed method makes

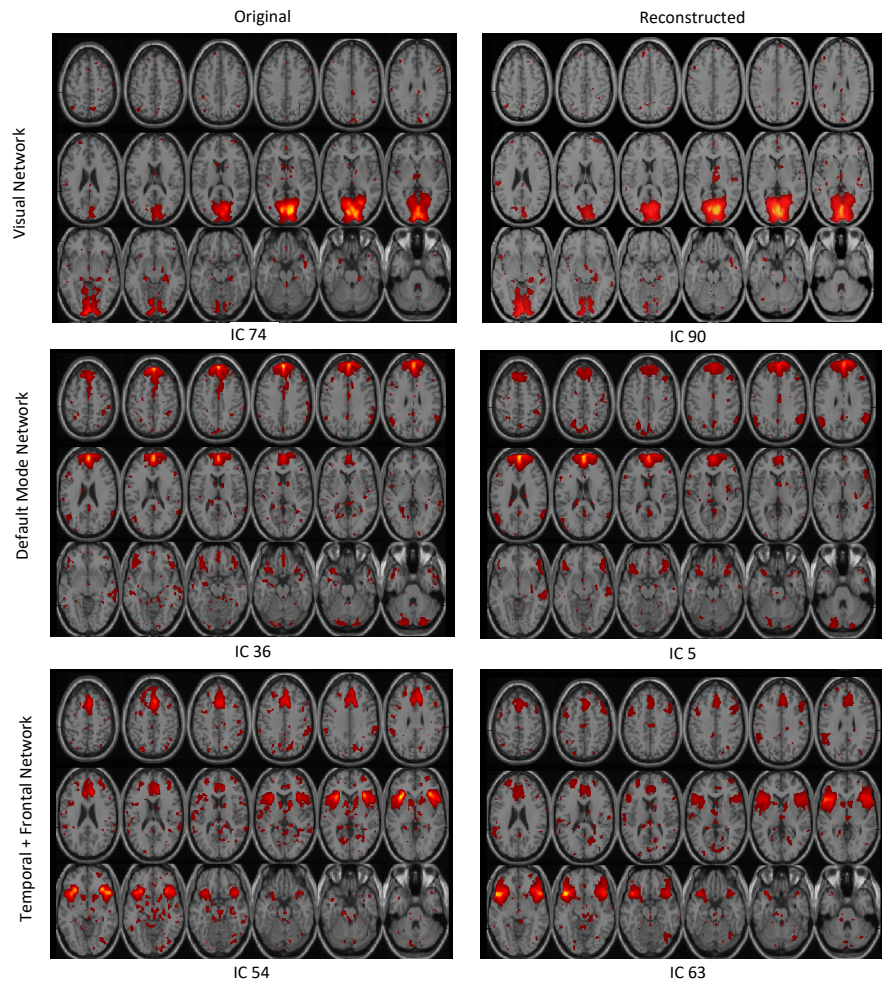


Figure 6: Axial view of spatial maps of various RSNs where the left part of each figure represents networks identified using the fully available (original) Beijing\_Zang data and the right part represents networks identified using the DTSR reconstructed data. Each row corresponds to results on one RSN. Number in brackets below each image represents independent component (IC) number obtained after group ICA.

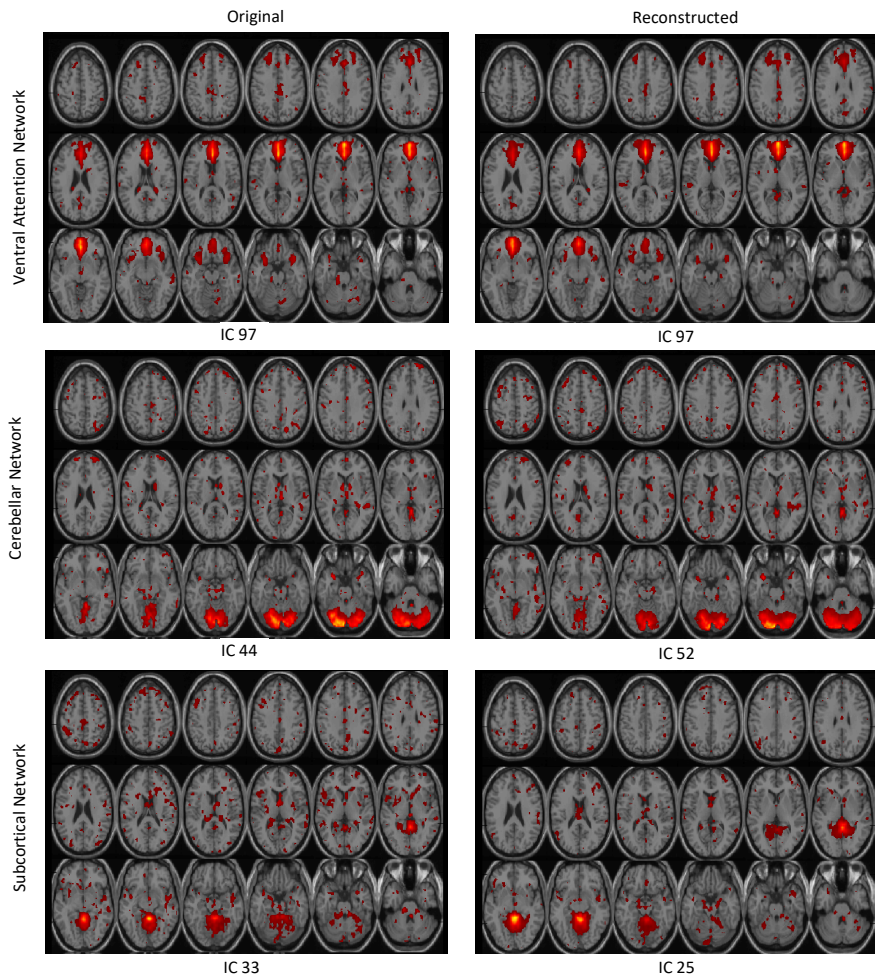


Figure 7: Axial view of spatial maps of various RSNs where the left part of each figure represents networks identified using the fully available (original) Beijing\_Zang data and the right part represents networks identified using the DTSR reconstructed data. Number in brackets below each image represents independent component (IC) number obtained after group ICA.

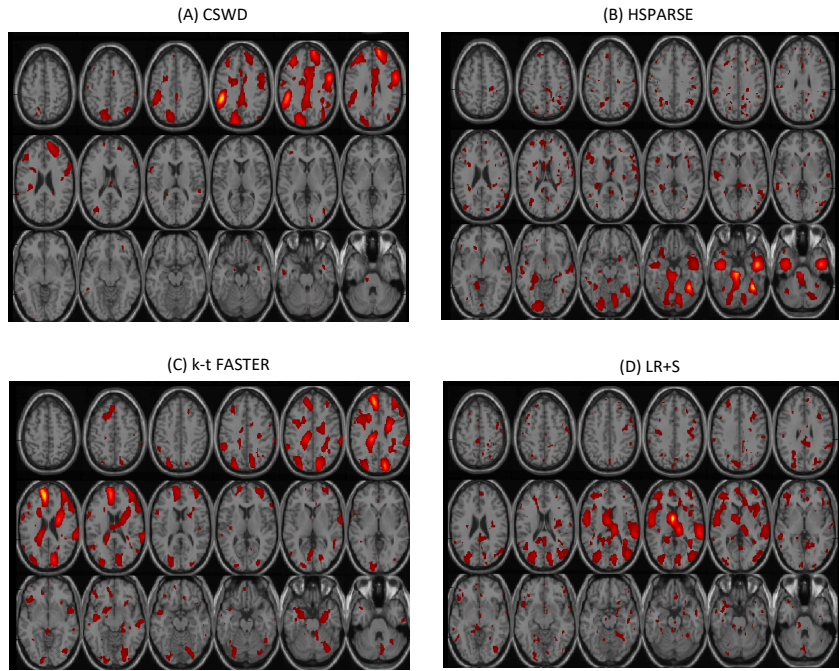


Figure 8: Axial view of one random spatial map obtained from the data reconstructed using (A) CSWD; (B) HSPARSE; (C)  $k-t$  FASTER; and (D) LR+S.

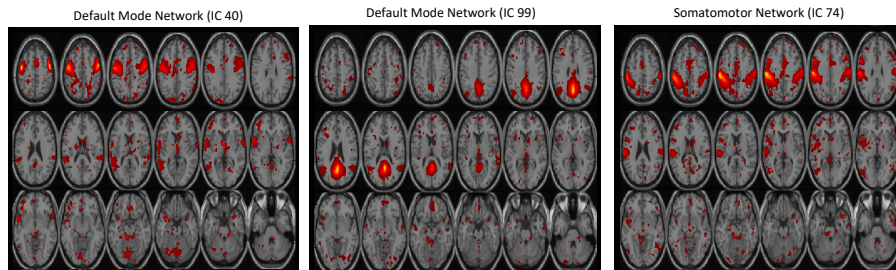


Figure 9: Axial view of spatial maps of various ICs obtained from the DTSR reconstructed data

use of the advantage of repeated scanning of the same brain volume in fMRI to study brain’s function. Scanning of the same brain volume over time brings similarity in the temporal direction that can be utilized via total variation based regularization. In addition to this, we also imposed conventional temporal sparsity in the proposed reconstruction framework and hence, name the proposed method as Double Temporal Sparsity based Reconstruction (DTSR).

Compressed sensing is used to recover undersampled data captured at different acceleration factors, although inherently weak BOLD signals in resting state fMRI prohibits the use of higher acceleration factors [17, 21]. However, in this work, we have been able to achieve robust and reproducible results with a higher acceleration factor of 12.856 (corresponding to 6 radial lines). In addition, results at lower acceleration factors are improved compared to the existing methods [19, 20, 21, 22].

We have thoroughly evaluated the robustness and the feasibility of the proposed DTSR method both at the subject and the group levels of fMRI data. The performance of DTSR method has been evaluated using retrospective undersampling of the fully available fMRI dataset. We compared the performance of the proposed method with other offline methods such as Compressed Sensing with Wavelet domain Sparsity (CSWD) [19], HSPARSE [20],  $k$ - $t$  FASTER [21], and LR+S [22]. Reconstruction reliability increases with increasing number of radial lines (lower acceleration factors). Table 1 and 2 show that error increases with decreasing number of radial lines. However, the proposed DTSR method is equally reliable at lower number of radial lines, i.e., at higher acceleration factors. Comparison with other methods shows that DTSR method produces lowest error (0.0471) at a high acceleration factor of 12.856 (corresponding to 6 radial lines). Further, results presented in Fig.5 demonstrate that the existing reconstruction methods produce greater artifact at this high acceleration factor.

The robustness and the reliability of the proposed method are further assessed using both quantitative and qualitative analyses on fMRI data. Results from the quantitative analysis show that the NMSE of the proposed reconstruction method is less compared to that of the other reconstruction methods (Table 1). Thus, it is noted that the incorporation of total variation along with sparsity as used in the proposed DTSR method improves reconstruction results significantly. The proposed DTSR reconstruction method produces significantly high values of PSNR and SSIM, and lower values of NMSE compared to the other existing methods (Table 1 and 2).

Two observations are in order from the qualitative results (Fig.5-6): (i) intrinsic resting state networks are consistent and comparable to the fully sampled fMRI data. Hence, crude estimate of regularization parameters is sufficient for reconstruction; and (ii) the fidelity of the proposed method in maintaining temporal information is established via consistency of results and via observation of all RSNs.

In summary, the proposed DTSR reconstruction method maintains temporal resolution even at higher acceleration factors without affecting the spatial resolution and can be used to provide accelerated fMRI reconstruction with accurate detection of intrinsic brain’s Resting State Networks (RSNs). Moreover,

the proposed DTSR method is able to improve BOLD sensitivity both at the individual and at the group level compared to the existing methods.

#### *Limitations and Future Work*

This work has proposed DTSR reconstruction method that exhibits better accelerated reconstruction performance compared to the existing methods using radial sampling pattern. However, 3D radial Cartesian sampling grid is more practical from the point of view of compressed data acquisition in scanner [21]. In future, we will use realistic sampling patterns to undersample data.

Secondly, use of both parallel imaging and CS fMRI may give excellent high spatio-temporal fMRI quality such as that observed in the context of dynamic MRI [47, 48, 49]. Thus, further studies may be undertaken to enhance the performance of DTSR method by using it in conjunction with existing parallel fMRI imaging methods [11, 12].

Thirdly, CS has been widely used to improve fMRI acquisition time. Hence, using this in conjunction with other high spatial resolution techniques, such as super-resolution technique [50] or simultaneous multi-slice imaging [51], may provide high spatio-temporal fMRI [20]. In the future, we will explore accelerated reconstruction from the perspective of improving spatial resolution.

Fourth, time complexity of DTSR is high because it involves multiplication of large  $\mathbf{X}$  and  $\mathbf{D}$  matrices. In the future, we will use GPU based computation to lower the computational time complexity.

Fifth, currently the manuscript is positioned on fMRI signal reconstruction. However, the detailed analysis and comparison of reconstructed data based ICA maps, such as automatic ICA selection, functional connectivity learning have not been explored in this paper. We will do rigorous qualitative analysis in our future works that would be actually positioned on building functional brain networks from fMRI data.

Finally, further evaluation of the proposed method on prospective undersampled fMRI data will help to check its robustness in real scenarios. In the future, we would also like to explore the performance of the proposed DTSR method on task-based fMRI data in order to understand the role of total variation and temporal sparsity in the accelerated reconstruction.

## **5. Conclusions**

In this paper, we have introduced a novel accelerated fMRI reconstruction method that exploits the advantage of scanning the same brain volumes in fMRI over a number of time points via double temporal sparsity constraints. The proposed DTSR reconstruction method can be used to acquire high temporal resolution fMRI data in smaller times comparable to those of lower resolution fMRI data along with accurate detection of intrinsic resting state brain networks. The performance of the proposed method has been evaluated using retrospective undersampling of the fully available real fMRI dataset of resting state. In the future, we would like to explore the performance of this method on task-based

fMRI data. Code of proposed DTSR method can be obtained from (<http://in.mathworks.com/matlabcentral/fileexchange/63768-dtsr-fmri-reconstruction>).

### Acknowledgements

The first author would like to thank Visvesvaraya research fellowship, Department of Electronics and Information Tech., Ministry of Comm. and IT, Govt. of India, for providing financial support for this work.

### References

- [1] N. K. Logothetis, What we can do and what we cannot do with fMRI, *Nature* 453 (7197) (2008) 869–878, ISSN 0028-0836.
- [2] D. A. Feinberg, E. Yacoub, The rapid development of high speed, resolution and precision in fMRI, *NeuroImage* 62 (2) (2012) 720–725, ISSN 1053-8119.
- [3] S. Ogawa, T. M. Lee, A. R. Kay, D. W. Tank, Brain magnetic resonance imaging with contrast dependent on blood oxygenation., *Proc Natl Acad Sci USA* 87 (24) (1990) 9868–9872, ISSN 0027-8424.
- [4] T. Q. Duong, E. Yacoub, G. Adriany, X. Hu, K. Ugurbil, J. T. Vaughan, H. Merkle, S.-G. Kim, High-resolution, spin-echo BOLD, and CBF fMRI at 4 and 7 T, *Magn Reson Med* 48 (4) (2002) 589–593, ISSN 1522-2594.
- [5] E. Yacoub, T. Q. Duong, P.-F. Van De Moortele, M. Lindquist, G. Adriany, S.-G. Kim, K. Uurbil, X. Hu, Spin-echo fMRI in humans using high spatial resolutions and high magnetic fields, *Magn Reson Med* 49 (4) (2003) 655–664, ISSN 1522-2594.
- [6] N. Harel, Ultra high resolution fMRI at ultra-high field, *NeuroImage* 62 (2) (2012) 1024–1028, ISSN 1053-8119.
- [7] E. Yacoub, N. Harel, K. Uurbil, High-field fMRI unveils orientation columns in humans, *Proc Natl Acad Sci USA* 105 (30) (2008) 10607–10612.
- [8] N. K. Logothetis, H. Merkle, M. Augath, T. Trinath, K. Ugurbil, Ultra High-Resolution fMRI in Monkeys with Implanted RF Coils, *Neuron* 35 (2) (2002) 227–242, ISSN 0896-6273.
- [9] J. Pfeuffer, P.-F. van de Moortele, E. Yacoub, A. Shmuel, G. Adriany, P. Andersen, H. Merkle, M. Garwood, K. Ugurbil, X. Hu, Zoomed Functional Imaging in the Human Brain at 7 Tesla with Simultaneous High Spatial and High Temporal Resolution, *NeuroImage* 17 (1) (2002) 272–286, ISSN 1053-8119.
- [10] P.-H. Wu, P.-H. Tsai, M.-L. Wu, T.-C. Chuang, Y.-Y. Shih, H.-W. Chung, T.-Y. Huang, High spatial resolution brain functional MRI using sub-millimeter balanced steady-state free precession acquisition, *Med Phys* 40 (12) (2013) 122304–122316.

- [11] T. Hugger, B. Zahneisen, P. LeVan, K. J. Lee, H.-L. Lee, M. Zaitsev, J. Hennig, Fast Undersampled Functional Magnetic Resonance Imaging Using Nonlinear Regularized Parallel Image Reconstruction, *PLoS One* 6 (12) (2011) 1–9.
- [12] L. Chaari, P. Ciuciu, S. Mériaux, J.-C. Pesquet, Spatio-temporal wavelet regularization for parallel MRI reconstruction: application to functional MRI, *Magn Reson Mater Phy* 27 (6) (2014) 509–529, ISSN 1352-8661.
- [13] W. Lu, T. Li, I. Atkinson, N. Vaswani, Modified-CS-residual for recursive reconstruction of highly undersampled functional MRI sequences, in: *Proc Int Conf Image Process*, ISSN 1522-4880, 2689–2692, 2011.
- [14] S. Yan, L. Nie, C. Wu, Y. Guo, Linear Dynamic Sparse Modelling for functional MR imaging, *Brain Inform* 1 (1) (2014) 11–18, ISSN 2198-4018.
- [15] P. K. Han, S.-H. Park, S.-G. Kim, J. C. Ye, Compressed sensing for fMRI : feasibility study on the acceleration of non-EPI fMRI at 9.4 T, *Biomed Res Int* 2015 (131926) (2015) 1–24.
- [16] H. Jung, J. C. Ye, Performance evaluation of accelerated functional MRI acquisition using compressed sensing, in: *Proc IEEE Int Symp Biomed Imaging*, ISSN 1945-7928, 702–705, 2009.
- [17] X. Zong, J. Lee, A. J. Poplawsky, S.-G. Kim, J. C. Ye, Compressed sensing fMRI using gradient-recalled echo and EPI sequences, *NeuroImage* 92 (2014) 312–321, ISSN 1053-8119.
- [18] C. Chavarrías, J. Abascal, P. Montesinos, M. Desco, Exploitation of temporal redundancy in compressed sensing reconstruction of fMRI studies with a prior-based algorithm (PICCS), *Med phys* 42 (7) (2015) 3814–3821.
- [19] D. J. Holland, C. Liu, X. Song, E. L. Mazerolle, M. T. Stevens, A. J. Sederman, L. F. Gladden, R. C. N. D’Arcy, C. V. Bowen, S. D. Beyea, Compressed sensing reconstruction improves sensitivity of variable density spiral fMRI, *Magn Reson Med* 70 (6) (2013) 1634–1643, ISSN 1522-2594.
- [20] Z. Fang, N. Van Le, M. Choy, J. H. Lee, High spatial resolution compressed sensing (HSPARSE) functional MRI, *Magn Reson Med* 76 (2) (2016) 440–455, ISSN 1522-2594.
- [21] M. Chiew, N. N. Graedel, J. A. McNab, S. M. Smith, K. L. Miller, Accelerating functional MRI using fixed-rank approximations and radial-cartesian sampling, *Magn Reson Med* 76 (6) (2016) 1825–1836, ISSN 1522-2594.
- [22] V. Singh, A. Tewfik, D. Ress, Under-sampled functional MRI using low-rank plus sparse matrix decomposition, in: *Proc IEEE Int Conf Acoust Speech Signal Process*, ISSN 1520-6149, 897–901, 2015.

- [23] D. Donoho, Compressed sensing, *IEEE Trans. Inf. Theory* 52 (4) (2006) 1289–1306, ISSN 0018-9448.
- [24] P. Aggarwal, P. Shrivastava, T. Kabra, A. Gupta, Optshrink LR+S: accelerated fMRI reconstruction using non-convex optimal singular value shrinkage, *Brain Inform* 4 (1) (2017) 65–83, ISSN 2198-4026.
- [25] P. Aggarwal, A. Gupta, Accelerated fMRI reconstruction using Matrix Completion with Sparse Recovery via Split Bregman, *Neurocomputing* 216 (2016) 319–330, ISSN 0925-2312.
- [26] E. Candes, J. Romberg, T. Tao, Robust uncertainty principles: exact signal reconstruction from highly incomplete frequency information, *IEEE Trans. Inf. Theory* 52 (2) (2006) 489–509, ISSN 0018-9448.
- [27] Y. Wang, J. Yang, W. Yin, Y. Zhang, A new alternating minimization algorithm for total variation image reconstruction, *SIAM J Imaging Sci* 1 (3) (2008) 248–272.
- [28] B. B. Biswal, M. Mennes, X.-N. Zuo, S. Gohel, C. Kelly, S. M. Smith, C. F. Beckmann, J. S. Adelstein, R. L. Buckner, S. Colcombe, et al., Toward discovery science of human brain function, *Proc Natl Acad Sci USA* 107 (10) (2010) 4734–4739.
- [29] S. Boyd, N. Parikh, E. Chu, B. Peleato, J. Eckstein, Distributed optimization and statistical learning via the alternating direction method of multipliers, *Found Trends Mach Learn* 3 (1) (2011) 1–122.
- [30] Y. Chen, J. A. O’Sullivan, D. G. Politte, J. D. Evans, D. Han, B. R. Whiting, J. F. Williamson, Line Integral Alternating Minimization Algorithm for Dual-Energy X-Ray CT Image Reconstruction, *IEEE Trans Med Imaging* 35 (2) (2016) 685–698, ISSN 0278-0062.
- [31] R. P. Monti, P. Hellyer, D. Sharp, R. Leech, C. Anagnostopoulos, G. Montana, Estimating time-varying brain connectivity networks from functional MRI time series, *NeuroImage* 103 (2014) 427–443, ISSN 1053-8119.
- [32] A. Gogna, A. Shukla, H. K. Agarwal, A. Majumdar, Split Bregman algorithms for sparse / joint-sparse and low-rank signal recovery: Application in compressive hyperspectral imaging, in: *Proc Int Conf Image Process*, ISSN 1522-4880, 1302–1306, 2014.
- [33] P. Aggarwal, A. Gupta, A. Garg, Multivariate brain network graph identification in functional MRI, *Medical Image Analysis* 42 (2017) 228–240, ISSN 1361-8415.
- [34] Y. Zheng, X. Zhang, S. Yang, L. Jiao, Low-rank representation with local constraint for graph construction, *Neurocomputing* 122 (2013) 398–405, ISSN 0925-2312.

- [35] S. G. Lingala, Y. Hu, E. DiBella, M. Jacob, Accelerated dynamic MRI exploiting sparsity and low-rank structure: kt SLR, *IEEE Trans Med Imaging* 30 (5) (2011) 1042–1054.
- [36] S. Zhang, K. T. Block, J. Frahm, Magnetic resonance imaging in real time: Advances using radial FLASH, *J Magn Reson Imaging* 31 (1) (2010) 101–109, ISSN 1522-2586.
- [37] P. C. Hansen, Analysis of Discrete Ill-posed Problems by Means of the L-curve, *SIAM Rev* 34 (4) (1992) 561–580, ISSN 0036-1445.
- [38] M. Lustig, D. Donoho, J. M. Pauly, Sparse MRI: The application of compressed sensing for rapid MR imaging, *Magn Reson Med* 58 (6) (2007) 1182–1195.
- [39] Z. Wang, A. Bovik, Mean squared error: Love it or leave it? A new look at Signal Fidelity Measures, *IEEE Signal Process Mag* 26 (1) (2009) 98–117, ISSN 1053-5888.
- [40] V. D. Calhoun, V. K. Potluru, R. Phlypo, R. F. Silva, B. A. Pearlmutter, A. Caprihan, S. M. Plis, T. Adali, Independent component analysis for brain fMRI does indeed select for maximal independence, *PLoS One* 8 (8) (2013) e73309.
- [41] E. A. Allen, E. Damaraju, S. M. Plis, E. B. Erhardt, T. Eichele, V. D. Calhoun, Tracking Whole-Brain Connectivity Dynamics in the Resting State, *Cereb Cortex* 24 (3) (2014) 663–676.
- [42] V. Kiviniemi, T. Starck, J. Remes, X. Long, J. Nikkinen, M. Haapea, J. Veijola, I. Moilanen, M. Isohanni, Y.-F. Zang, et al., Functional segmentation of the brain cortex using high model order group PICA, *Hum Brain Mapp* 30 (12) (2009) 3865–3886.
- [43] A. Abou-Elseoud, T. Starck, J. Remes, J. Nikkinen, O. Tervonen, V. Kiviniemi, The effect of model order selection in group PICA, *Hum Brain Mapp* 31 (8) (2010) 1207–1216.
- [44] S. M. Smith, P. T. Fox, K. L. Miller, D. C. Glahn, P. M. Fox, C. E. Mackay, N. Filippini, K. E. Watkins, R. Toro, A. R. Laird, et al., Correspondence of the brain’s functional architecture during activation and rest, *Proc Natl Acad Sci USA* 106 (31) (2009) 13040–13045.
- [45] A. J. Bell, T. J. Sejnowski, An information-maximization approach to blind separation and blind deconvolution, *Neural Comput* 7 (6) (1995) 1129–1159.
- [46] F. Esposito, E. Formisano, E. Seifritz, R. Goebel, R. Morrone, G. Tedeschi, F. Di Salle, Spatial independent component analysis of functional MRI time-series: To what extent do results depend on the algorithm used?, *Hum Brain Mapp* 16 (3) (2002) 146–157.

- [47] J. Tsao, P. Boesiger, K. P. Pruessmann, k-t BLAST and k-t SENSE: Dynamic MRI with high frame rate exploiting spatiotemporal correlations, *Magn Reson Med* 50 (5) (2003) 1031–1042.
- [48] J. Tsao, S. Kozerke, P. Boesiger, K. P. Pruessmann, Optimizing spatiotemporal sampling for k-t BLAST and k-t SENSE: Application to high-resolution real-time cardiac steady-state free precession, *Magn Reson Med* 53 (6) (2005) 1372–1382.
- [49] F. Huang, J. Akao, S. Vijayakumar, G. R. Duensing, M. Limkeman, k-t GRAPPA: A k-space implementation for dynamic MRI with high reduction factor, *Magn Reson Med* 54 (5) (2005) 1172–1184.
- [50] E. Van Reeth, I. W. K. Tham, C. H. Tan, C. L. Poh, Super-resolution in magnetic resonance imaging: A review, *Concepts in Magnetic Resonance Part A* 40A (6) (2012) 306–325.
- [51] D. A. Feinberg, K. Setsompop, Ultra-fast MRI of the human brain with simultaneous multi-slice imaging, *Journal of Magnetic Resonance* 229 (2013) 90 – 100, *frontiers of In Vivo and Materials MRI Research*.